International Journal of Nanomedicine

Dovepress
open access to scientific and medical research

Open Access Full Text Article

ORIGINAL RESEARCH

Electrospun Icariin-Loaded Core-Shell Collagen, Polycaprolactone, Hydroxyapatite Composite Scaffolds for the Repair of Rabbit Tibia Bone Defects

This article was published in the following Dove Press journal:
International Journal of Nanomedicine

Hongbin Zhao[1]
Junjie Tang[1]
Dong Zhou[1]
Yiping Weng[1]
Wen Qin[1]
Chun Liu[1]
Songwei Lv[2]
Wei Wang[3]
Xiubo Zhao[2,4]

[1]Medical Research Centre, Changzhou Second People's Hospital Affiliated to Nanjing Medical University, Changzhou 213164, People's Republic of China; [2]School of Pharmaceutical Engineering and Life Science, Changzhou University, Changzhou 213164, People's Republic of China; [3]Medical School, Hexi University, Zhangye 730041, People's Republic of China; [4]Department of Chemical and Biological Engineering, University of Sheffield, Sheffield S1 3JD, UK

Background: Electrospinning is a widely used technology that can produce scaffolds with high porosity and surface area for bone regeneration. However, the small pore sizes in electrospun scaffolds constrain cell growth and tissue-ingrowth. In this study, novel drug-loading core-shell scaffolds were fabricated via electrospinning and freeze drying to facilitate the repair of tibia bone defects in rabbit models.

Materials and Methods: The collagen core scaffolds were freeze-dried containing icariin (ICA)-loaded chitosan microspheres. The shell scaffolds were electrospun using collagen, polycaprolactone and hydroxyapatite materials to form CPH composite scaffolds with the ones containing ICA microspheres named CPHI. The core-shell scaffolds were then cross-linked by genipin. The morphology, microstructure, physical and mechanical properties of the scaffolds were assessed. Rat marrow mesenchymal stem cells from the wistar rat were cultured with the scaffolds. The cell adhesion and proliferation were analysed. Adult rabbit models with tibial plateau defects were used to evaluate the performance of these scaffolds in repairing the bone defects over 4 to 12 weeks.

Results: The results reveal that the novel drug-loading core-shell scaffolds were successfully fabricated, which showed good physical and chemical properties and appropriate mechanical properties. Furthermore, excellent cells attachment was observed on the CPHI scaffolds. The results from radiography, micro-computed tomography, histological and immunohistochemical analysis demonstrated that abundant new bones were formed on the CPHI scaffolds.

Conclusion: These new core-shell composite scaffolds have great potential for bone tissue engineering applications and may lead to effective bone regeneration and repair.

Keywords: icariin (ICA), electrospinning, polycaprolactone, collagen 1, hydroxyapatite, bone regeneration

Introduction

Treatment of bone defects that caused by trauma, fracture, tumour, or infection, is still a major challenge in orthopedic practice.[1] Autografts and allografts although have been applied for many years, while it faces many disadvantages such as the limited supply, new trauma, and risk of disease transmission.[2,3] Due to the drawbacks of the traditional therapeutic approaches, as an alternative, bone tissue engineering (BTE) has drawn great attention as a new strategy for bone regeneration.[4,5]

Correspondence: Hongbin Zhao; Xiubo Zhao
Email zhao761032@163.com; xiubo.zhao@sheffield.ac.uk

submit your manuscript | www.dovepress.com
DovePress
http://doi.org/10.2147/IJN.S238800

The key components for BTE are scaffolds, cells and growth factors, among which fabrication of scaffolds that are suitable for BTE has been crucially important for cell attachment, migration, proliferation and differentiation.[6,7] Appropriate BTE scaffolds should have 1) excellent mechanical properties to ensure the bone tissue remodelling; 2) extracellular matrix (ECM) like chemical composition to facilitate cell attachment and proliferation; 3) excellent biocompatibility and biodegradability with controllable degradation and resorption rates to match the bone regeneration; 4) appropriate porosity for cells to attach, migrate, proliferate and deposit ECM.[8] Interconnection of pores is also required to allow the transportation of nutrients, metabolites and waste products removal.[9,10]

In the past decades, various synthetic and natural polymers and mineral materials have been explored as BTE scaffolds to mimic the natural bone tissues.[6,11] Bone is made primarily of hydroxyapatite (HA) crystals interspersed in a collagen (COL) matrix with HA accounting for 70% (by weight) of human bone.[12] Collagen is the main ECM protein in the body, and has excellent biocompatibility, therefore has been extensively used in tissue engineering applications. However, collagen scaffolds themselves are limited for use in orthopedic applications due to their poor mechanical properties.[8,13] Therefore, HA/collagen composite scaffolds have been extensively studied.[14,15] To take advantages of distinct properties of both materials for tissue-engineering construct development. For example, Cunniffe et al[8] have recently explored the use of nano-HA particles to fabricate the biomimetic-inspired scaffolds through the combination of collagen. It was found that increasing the composition of HA resulted in the increasing of Young's modulus of the scaffolds. The bioactive responses, cellular attachment and osteogenesis were enhanced. Earlier expression of bone markers and cell-mediated mineralization were also observed.[8]

HA possess characterstics of high specific strength and toughness, binders are required to glue the HA particles and form the scaffolds with enhanced properties. Although HA/collagen scaffolds provided better mechanical property compared to collagen scaffolds themselves, the mechanical property can be further enhanced by incorporating a polymer binder. Biodegradable polymers such as poly-L-lactic Acid (PLLA), polyglycolic acid (PGA), polylactic acid (PLA) and poly (lactic-co-glycolic) acid (PLGA) have been widely used in BTE.[16–19] However, individual polymer cannot provide desired properties for BTE applications. They are normally combined with HA or other mineral materials and serve as a glue to reinforce the mechanical property and also regulate the degradation of the scaffolds.[20] Among these polymers, PCL has better mechanical properties and appropriate degradation rate for bone regeneration.[6,10,21] For example, using 3D printing technology, Luo et al[7] have fabricated PCL/oyster shell powder (OSP) scaffolds for BTE. OSP particles were found dispersed in the polymer matrix and helped to improve the biomineralization of the scaffolds, which also improved the proliferation and differentiation of MG-63 cells. The addition of OSP in the scaffolds was found enhanced the osteogenic properties and cellular responses. Meanwhile, Shkarina et al[10] have recently explored silicate-containing hydroxyapatite (SiHA)/PCL composite scaffolds for BTE. Increased cell viability was observed with the SiHA/PCL composite scaffolds. However, high hydrophobicity of the PCL leads to poor cell attachment.[7,10] ECM and growth factors are normally required to facilitate the osteogenesis.[8,10] Growth factors, such as transforming growth factor-α (TGF-α), bone morphogenetic protein (BMP), insulin like growth factor etc., play a vital role in bone regeneration.[22–24] However, the high cost of these growth factors limited their widespread use, particularly in BTE practice.[25–27] In order to promote bone regeneration and repair, there is an urgent demand to find safe and low-cost alternatives.[27,28] Herba Epimedii (HEP) is a widely used traditional Chinese herb to treat osteoporosis in clinic.[29] Icariin (ICA), the major pharmacologically active compound of HEP, has been used as a potential enhancer of fracture healing, and reduce bone losing.[30–32] Therefore, ICA has a great potential as a growth factor alternative for BTE. Based on the above, combining PCL/collagen/HA together with addition of ICA provides a promising solution for BTE scaffold fabrication with HA providing the mechanical property, collagen facilitating the cell attachment and proliferation, while the PCL bonds the HA and collagen to enhance the mechanical property and regulate the degradation and ICA increases the osteoconductivity.

Chitosan is not only noncytotoxic and biodegradable but it also exhibits excellent biocompatible properties.[33,34] Due to the presence of abundant amino groups, chitosan carries a positive charge and thus reacts with negatively charged polymers.[35] It has been reported the use of chitosan in the formation of gels, nanoparticles, and microspheres for drug delivery application, because of their ability for sustained release and improved bioavailability of target molecules.[36,37]

Therefore, chitosan together with the advance of nanotechnology can be effectively applied as a carrier system for drug delivery, which can be a better option for bone tissue engineering.

Electrospinning is one of the widely used techniques to produce nanofibers for various tissue engineering.[38–40] Electrospun scaffolds possess high surface area to volume ratio and high porosity which can potentially mimic the natural ECM of bone tissues.[41,42] However, the small pore sizes in electrospun scaffolds restrain cell growth and tissue-ingrowth, how to increase the pore sizes in electrospun scaffolds is a new challenge in the future.[43–45]

The aim of this study was to design a new kind of core-shell scaffold is to mimic natural bone. It was hypothesized that such type of scaffold can satisfy both of mechanical and osteoinductive requirements for bone tissue regeneration. For this purpose, the structure of the shell scaffold that were fabricated by electrospinning with PCL/collagen/HA is compact, which is similar to cortical bone. Meanwhile, the core scaffolds that contained icariin (ICA)-loaded chitosan microspheres were fabricated by freeze-drying technologies using the combination of collagen, which can mimic the cancellous bone (Scheme 1). It was supposed that this kind of scaffold could improve the ability of bone regeneration.

Materials and Methods

Preparation of ICA Loaded Microspheres and in vitro Drug Release

To prepare the ICA loaded microspheres, 250 mg chitosan was dissolved in 10 mL of 2% acetic acid. The sample was stirred using a hot plate at room temperature for 24 h until a homogeneous solution was obtained. After this, 40 mg ICA (Purity ≥ 99.8%, from Chinese Institute for Drug Assay, Beijing, China) was blended into the chitosan solution to form a homogeneous mixed solution at room temperature. Finally, the mixed solution was added dropwise (5 mL/h) into a 100 mL paraffine solution containing 2% Span-80 before the addition of 25 mL (5%) tripolyphosphate solution. The sample was being continuously stirred (450 rpm) on a hot plate until the stable drug loaded microspheres were formed. The supernatant was then removed through centrifugation (2000 rpm for 30 min) and the microspheres were rinsed for three times with ligroin and isopropanol,

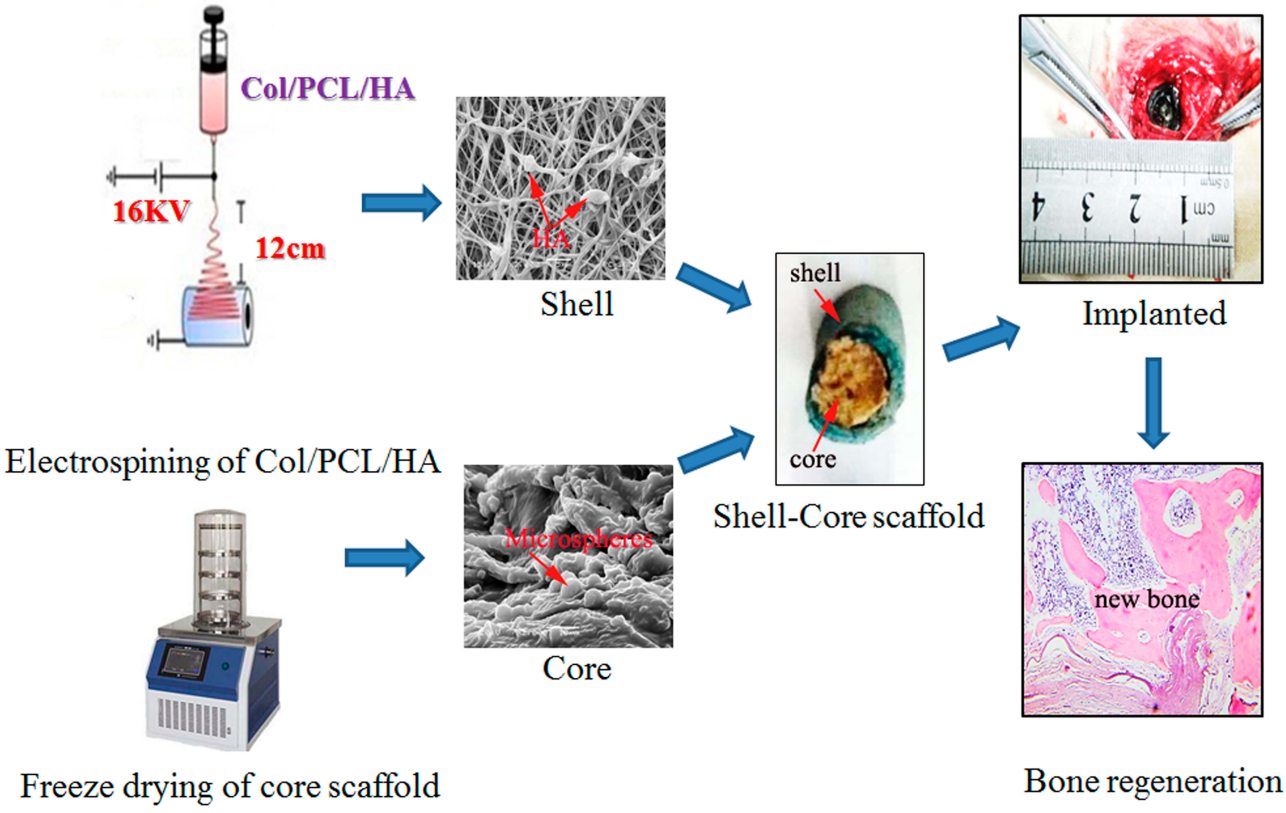

Scheme 1 Schematic illustration of the fabrication process of PCL/COL/HA/ICA composite scaffold.

respectively, before freeze-drying for 12 h. Meanwhile, the ICA-unloaded microspheres were also prepared as control using the same method.

For the drug release assay, a total of 30 mg of chitosan microspheres were placed into a dialysis bag and left in 100 mL PBS (pH = 7.4, 0.01 M). The sample was incubated under constant shaking at 37 °C and, 1 mL supernatant was collected for each time at selected time scales (1 d, 3 d, 5 d, 15 d, 20 d to 60 d), an equal volume of fresh PBS was added. The ICA-unloaded microspheres in PBS were also incubated at 37 °C as control. The amount of ICA release in PBS buffer was tested by UV spectrophotometer at 270 nm.

Fabrication of CPH and CPHI Composite Scaffolds

Shell Scaffolds

To prepare the electrospun nanofibrous scaffolds, 0.3 g collagen 1 (COL1), 0.3 g polycaprolactone (PCL, Sigma-Aldrich, USA, molecular weight, 80,000) and 0.1 g hydroxyapatite (HA) were dissolved in hexafluoroisopropanol (HFLP, Sigma-Aldrich, USA) to form a 3% (w/v) to form a homogeneous solution. The electrospinning was carried out at a voltage of 15 kV and a flow rate of 1 mL/h using a DT −1003 electrospinning (Dalian Dingtong tech. Ltd). The electrospun fibres were collected onto 10 mm diameter cylinder collectors at a distance of 12 cm from the syringe needle with the receiving shaft spinning at 530 rpm. The process was stopped when the thickness of the electrospun shell scaffolds increased to 0.7–0.8 mm. The samples were subsequently placed into a vacuum for 72 h at room temperature to remove HFLP solvent.

Core Scaffolds

To prepare the core scaffolds, COL1 was dissolved in 1% glacial acetic acid to form a 4% (w/v) homogeneous solution. 10 mL solution was then mixed with 30 mg microspheres, and stirred with a magnetic stirrer to form a uniform liquid. Meanwhile, unloaded-ICA microspheres were mixed for the fabrication as control scaffold. The mixtures were placed into a special circular mold (diameter 8 mm) then stored at −80 °C for 2 h before freeze drying for 24 h. Finally, the core scaffolds were incubated in 0.1% genipin (0.1 M PBS, pH = 7.4) at 37 °C for 1 h,[46] After neutralization by NaOH (0.01 M) at room temperature for 30 min, the samples were washed three times using DI water, then were dried at room temperature.

CPH and CPHI Composite Scaffolds

The core scaffold was placed into shell scaffold after they were cut into 20 mm length respectively. The shell scaffolds were electrospun using collagen (COL), polycaprolactone (PCL), hydroxyapatite (HA) materials and the core scaffold that incorporated the unloaded-ICA microspheres to form CPH composite scaffolds with the ones containing ICA microspheres named CPHI. Then the core scaffold was placed into shell scaffold before incubated in 1% genipin (0.1 M PBS, pH = 7.4) at 37 °C for 30 min. After neutralization by NaOH (0.01 M) at room temperature for 30 min, the samples were washed three times using DI water. Finally, the scaffold were obtained after being dried at room temperature for 12 h. Each scaffold was cut with a surgical knife blade to 5 mm in length, sealed, and sterilized with Co-60.

Water Absorption, Porosity, Contact Angles, and Degradation of the Scaffolds

The water-absorption capacities of scaffolds were determined by swelling the scaffolds in DI water at 37 °C. The scaffolds (5 mm in length and 10 mm in diameter) were separately immersed into DI water for 24 h. The water absorption ratio was obtained with the following equation:[47]

$$\text{Water absorption ratio}\,(\%) = \frac{W_H - W_D}{W_D} \times 100$$

where W_H is the weight of the soaked scaffold and W_D is the weight of the dry scaffold.

The porosity of the scaffolds was measured based on gravimetry according to the following equation:[48]

$$\text{Porosity}\,(\%) = \frac{M_2 - M_3 - M_S}{M_1 - M_{3D}} \times 100$$

where M_1 is the initial mass of a bottle filled with ethanol, M_s is the mass of the dry scaffold, M_2 is the mass of the scaffold submerged in absolute ethanol within the bottle, and M_3 is the mass of the bottle after the scaffold was gently removed.

Contact angles for the shell scaffold were measured using a contact angle analyzer (FTA125, First Ten Angstroms, Portsmouth, VA, USA). Samples of the shell scaffold were first cut into 1 cm^2 square pieces (n = 4) and then placed on a testing plate. Subsequently, 0.03 mL of DI water was carefully dropped onto the test sample surface. After 10 second, the contact angles were recorded by video monitor.

For assessment of scaffold degradation, cylindrical samples were cut into 10 mm in length. Samples were placed into vials containing 10 mL 0.01 M PBS (pH = 7.4), and the vials were placed in a shaking water bath at 37 °C for 4–8 weeks. The PBS solution was changed weekly. The loss in mass of the scaffold was then calculated using the following equation:[49]

$$\text{Weight lost}\,(\%) = \frac{M_0 - M_D}{M_0} \times 100$$

where M_0 is the initial weight of the scaffold and M_D is the dry weight after degradation.

FTIR Study of the Scaffolds

A total of 2 mg dried CPH or CPHI powder was mixed with 200 mg KBr and compressed into a disk. Fourier transform infrared spectroscopy (FTIR, AVATAR 360, NICOLET, USA) was used to evaluate the functional groups of the scaffolds. All spectra were obtained between 4000 and 400 cm^{-1} at a 4 cm^{-1} resolution with 32 scans. Six samples were examined for 3 times.

Mechanical Testing

Before testing, the scaffolds were cut so that the gauge length and diameter of all specimens were 20 mm and 10 mm, respectively. For assessment of tension strength, the scaffolds were tested with an Instron 4505 universal testing machine (Instron Pty Ltd., Norwood, MA, USA) at a rate of 5 mm/second. Stress-strain graphs were then drawn according to the load/break data.

Cell Isolation, Seeding and Proliferation

Rat marrow mesenchymal stem cells (rMSCs) were isolated from femurs obtained from wistar rats by flushing the bone marrow with PBS. The bone marrow cells were then washed three times in PBS by centrifugation (10 min, 250 × g). The cells obtained from rat femurs were subsequently cultured in DMEM/F12 (D/F12), contain 10% FBS and 1% antimycotic/antibiotic, in an incubator at 37 °C with 5% CO_2 and expanded over three passages. The scaffolds were pre-wetted in D/F12 in 24 well plates overnight. The cells (1×10^6 cells/mL) were suspended in 100 μL of D/F12 medium and seeded on scaffolds, and subsequently cultured in six-well plates for 2 h. 2 mL medium was then added into each well and consecutively cultured for 3, 7 and 14 d.

Scanning Electron Microscopy (SEM) and Fluorescence Staining

The microstructure of the scaffolds and the shape of drug microspheres were observed by SEM. At day 7, cell-seeded scaffolds were rinsed in PBS (pH = 7.4, 0.01 M) (n = 3), fixed in 2.5% glutaraldehyde for 48 h. Samples were dehydrated and sputter coated with gold as common practice for 10 min before SEM measurements. For fluorescence staining, the samples were dehydrated, and embedded in paraffin before stained with 3 μM 4′,6-diamidino-2-phenylindole, dihydrochloride (DAPI, Sigma, USA) for nucleus. Parallel samples were stained with hematoxylin-eosin (H&E). The samples were observed under a fluorescence and optical microscope (Olympus, Tokyo, Japan), respectively.

Animal Experiment Procedures

For examination of bone regeneration, the CPH and CPHI scaffolds were implanted into tibial plateau created in 60 male Japanese white rabbits (2 months old; weight: 1.5–2.0 kg) purchased from the Lanzhou Veterinary Research Institute of the Chinese Academy of Agricultural Science.

Rabbits were randomly divided into 3 groups ($N = 20$/group) for control, CPH and CPHI. All animals were anesthetized by intravenous injection of pentobarbital sodium (0.3 mL/kg). The tibial plateau of rabbits was exposed. The bone defect (10 mm in diameter, 5 mm in depth) was made in the tibial plateau by an electric drill. Bone debris was removed by physiologic saline irrigation. The CPH and CPHI scaffolds (CPH and CPHI group) were then implanted in the bone defect areas, respectively. In the control group, no scaffolds were implanted in the defect areas. The skin and musculature were sutured in layers. Using iodine wiped suture and marked. To prevent postoperative infections, penicillin injections (400k units) were administered once a day for 7 days. The general conditions of the rabbits (diet, activity, energy, and wound healing) were continuously monitored for 2 weeks.

Radiographic and Three-Dimensional CT Scanning

X-ray and three-dimensional CT were performed to analyse bone regeneration and reconstruction conditions. Rabbits (n = 3) from each group were anesthetized by pentobarbital at 4, 8, 12 weeks post-operation, respectively. The bone

defect areas were examined by X-ray and three-dimensional CT reconstruction scanning.

Micro-CT Scanning and Quantitative Analysis

After radiographic examination, the rabbits were anesthetized with an overdose of pentobarbital. The soft tissues attached to the bone defect were gently removed and the tibias were harvested and fixed in 10% formaldehyde for 48 h. The samples were scanned with high-resolution (12 μm) micro-CT (GE Healthcare, USA) and a 3D image was reconstructed before the measurement of the bone mineral density of new bone. 3 rabbits in each group were measured for three times, and the amount of bone regeneration was calculated based on the average value.

Histological Staining

20 mm bone tissue samples were collected from the tibia in each group, fixed in 10% formaldehyde for 72 h and subsequently decalcified in 5% EDTA-Na_2 (pH = 7.0) for 5 weeks at room temperature. After complete decalcification, the samples were dehydrated, and embedded in paraffin. Hematoxylin and eosin (H&E) staining and Masson trichrome staining were employed to analyse bone regeneration and scaffold degradation at bone defect areas. All histological images were photographed digitally with a microscope and analyzed with a digital image analysis system (DXM 1200, Nikon, Japan).

Immunohistochemical Staining

Samples were deparaffinized in ascending ethanol, then rehydrated by boiling in sodium citrate solution for 10 min. The immunohistochemical assay was performed following the protocols provided by the manual of the kit. Sections were reacted with the primary antibodies: mouse monoclonal alkaliphosphatase (ALP) antibody (1:500, overnight at 4 °C; Abcam, USA), rabbit monoclonal type I collagen (Col I), rabbit monoclonal osteocalcin (OCN) antibody (1:500, overnight, 4 °C; Abcam, USA) and rabbit monoclonal osteopontin (OPN) antibody (1:500, overnight, 4 °C; Abcam, USA). The biotinylated secondary antibody (1:1000, 37 °C, either goat anti-mouse or anti-rabbit) was applied for 30 min. Sections were stained with 3,3′-diaminobenzidine tetrahydrochloride (DAB, sigma, USA), rinsed with PBS (pH = 7.4, 0.02 M), dehydrated, and examined with a microscope (Olympus). All histological and immunohistochemical images were photographed digitally with a CCD camera and analyzed with a digital image analysis system (DXM 1200, Nikon, Japan).

Animal Study Approval

All animal studies were performed in compliance with the regulations and guidelines of the Orthopedics department and approved by China's Animal Research Authority and Ethics Committee of the General Hospital of Lanzhou Military Command of the PLA. Animal care was conducted according to the Association for Assessment and Accreditation of Laboratory Animal Care international (AAALAC) and Institutional Animal Care and Use Committee (IACUC) guidelines.

Statistical Analyses

All data are presented as means ± standard deviations. A two-tailed unpaired Student's *t*-test was used to assess for significant differences between groups; P value < 0.05 was considered statistically significant. SPSS 13.0 statistical software (SPSS, USA) was used to analyze all data.

Results

Scaffold Characterization

The morphology of the fabricated scaffolds were observed by scanning electron microscopy (SEM) as shown in (Figure 1A2-3 and B2-3). The shell scaffolds produced by electrospinning displayed three-dimensional network structure with high porosity. The mean diameters of the fibres in the uncross-linked scaffolds are in the range from 100 to 700 nm (Figure 1A2). However, when the scaffolds were cross-linked by genipin, the fibres diameters increased from 100–700 nm to 300–1000 nm (Figure 1B2). The surface of the fibres also became rough compared to the control group. The morphology of the core scaffolds were also observed by SEM. It was found that the microstructure of the uncross-linked core scaffolds was characterized by smooth surface topography (Figure 1A3). After cross-linking by genipin, the surface morphology was switched to be rough and compact. However the pore sizes and the number of pores were not significantly reduced in comparison with the uncross-linked scaffolds (Figure 1D).

The water absorption measurement of the scaffolds is shown in Figure 1C. It was found that uncross-linked scaffolds have a water absorption ratio of 48.6%. However, after cross-linking with genipin, the water absorption was reduced to 39.5%, indicating the decrease of the water absorption

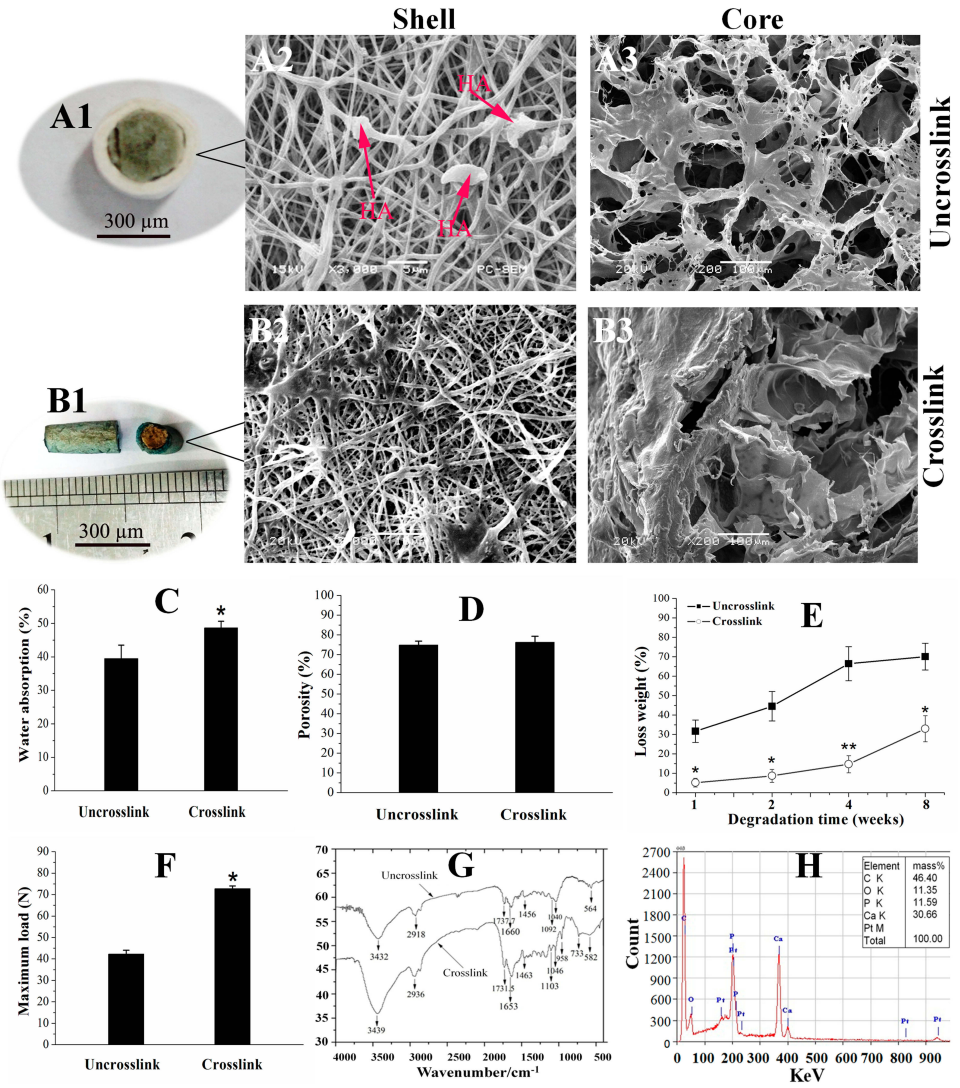

Figure 1 Surface topography and physical properties of the CPH scaffolds. (**A1**) The gross appearance of the uncross-linked scaffolds. (**A2**–**A3**) Scanning electron microscopy images of the uncross-linked scaffolds. (**B1**) The gross appearance of the cross-linked scaffolds. (**B2**–**B3**) Surface topography of the cross-linked scaffolds. (**C**) Water absorption ratios. (**D**)Porosity. (**E**) Loss weight; and mechanical property (**F**) of the scaffolds with and without cross-linking. (**G**) Spectra of the CPHI scaffolds with and without cross-linking. (**H**) Characterization of the hydroxyapatite (HA)-incorporated scaffolds. The results are presented as the mean ± standard deviations (n = 3). * $p < 0.05$; ** $p < 0.01$; * is the significance compared to the uncross-linked scaffolds.
Abbreviation: HA, hydroxyapatite.

after genipin cross-linking. As shown in Figure 1D, the porosity for the scaffold was 76.3% and 74.8% for the cross-linked scaffolds ones and uncross-linked scaffolds ones, respectively. Therefore, no significant difference between the two types of scaffolds was found. The degradation rate of the scaffolds that soaked in PBS for 8 weeks was 32.98% for the cross-linked scaffolds and 70.06% for the uncross-linked scaffolds (Figure 1E), indicating that the cross-linking has a significant effect to the degradability.

Figure 1F shows the compressive strength of the scaffolds. The average maximum load for the scaffolds were 72.8±1.3 N for the cross-linked scaffolds, and 42.3±1.7 N for the uncross-linked scaffolds, showing that the mechanical strength of the cross-linked scaffolds were remarkably increased compared to the uncross-linked scaffolds.

To investigate the cross-linking, FTIR has been employed with the data shown in Figure 1G. The spectroscopic analysis confirmed the formation of cross-linking through the addition of genipin, reflected by the emergence of the desired bands at their respective positions. For the uncross-linked shell, the band at 564 cm^{-1} represents the P-O bending vibration; the bands at 1040 cm^{-1} and 1092 cm^{-1} represent HA stretching vibrations; the band at

1660 cm^{-1} represents the C=O stretching vibration; the band at 1456 cm^{-1} represents the N-H absorption; the bands at 1730–1737 cm^{-1} represent the C=O stretching vibrations. The presence of these bands further confirms that HA, PCL and Col were successfully blended in the composite materials. In comparison, for the cross-linked shell, the band at 1103 cm^{-1} represents the C-O-C stretching vibrations and the band at 733 cm^{-1} represents the N-H bending vibration, The absorbance band at 1104 cm^{-1} and 1370 cm^{-1} significantly increased (Figure 1G), indicating that collagen was cross-linked with genipin.[50]

Figure 1H shows the chemical composition of CPH scaffold. Strong signals were detected for Ca, and P, indicating the existence of HA-incorporated in the scaffold.

Microspheres Characterization, Distributed and ICA Release Kinetics of Scaffolds

We employed the chitosan to form micro-particles for the ICA drug loading and release. The chitosan microspheres were prepared as described in section 2.1 with the morphologies of chitosan microspheres shown in Figure 2A. The microspheres showed spherical shape with smooth surface and no aggregation was observed. The particle sizes of microspheres were between 1–5 μm. The cumulative release of ICA from the microspheres was measured and shown in Figure 2B. The resulting release curve exhibited a increased at 5 d, at which time 30% of the total amount of ICA had been released from microspheres. From 10 d, ICA release was significantly increased. Stable release was maintained such that 70% of the loaded ICA had been released by 20 to 60 d.

Figure 2C shows the SEM images of core scaffold that without incorporation of microspheres. The microspheres distribution in the core scaffolds is showed in Figure 2D. It was found that the microspheres evenly distributed in the core scaffolds, ensuring the stably release of ICA from the microspheres with the degradation process of the core scaffolds.

Cell Morphology

To investigate the cell attachment behaviour, rMSCs were cultured on the shell and core scaffolds for 7 days, respectively. Figure 3A shows the SEM and histological staining images of the rMSCs on the shell scaffolds after being cultured for 7 days. The cells stretched along the surfaces of the shell scaffolds to form a well attached cell layer (Figure 3A1-A3). Cell morphology on the core scaffolds

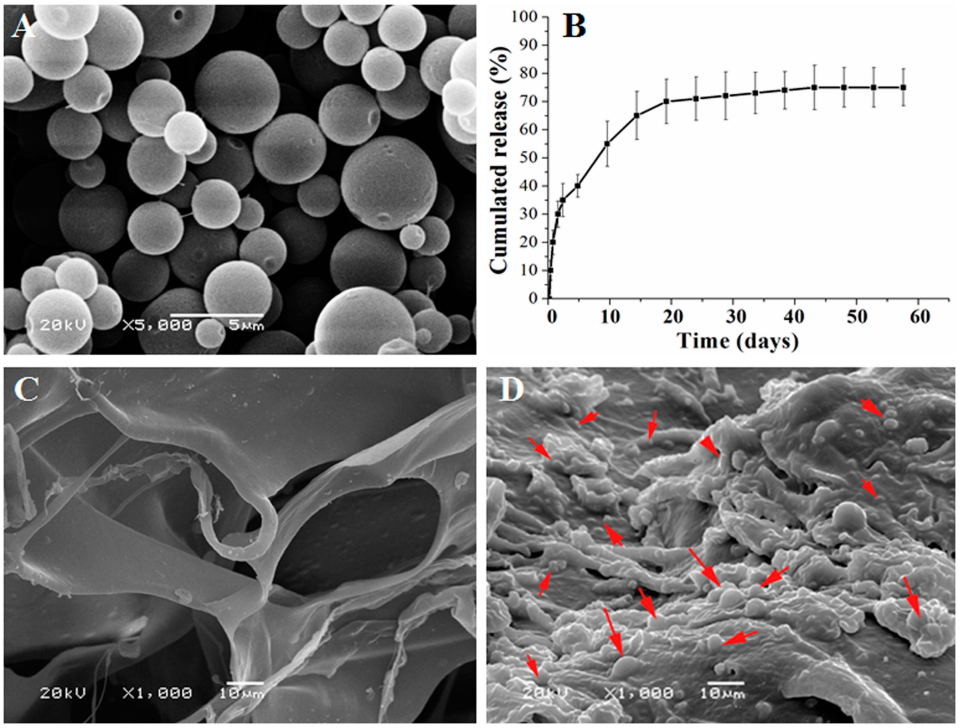

Figure 2 Characterization of microspheres, cumulative release of ICA and distribution. (**A**) Scanning electron microscopy images of the ICA loaded chitosan microspheres. (**B**) The curve of ICA released from the microspheres. (**C**) and (**D**) The scaffolds scanning electron microscopy images of the core scaffold, (**C**) without the chitosan microspheres, (**D**) with the chitosan microspheres. The results are presented as the mean ± standard deviations (n = 3). Red arrow: chitosan microspheres.

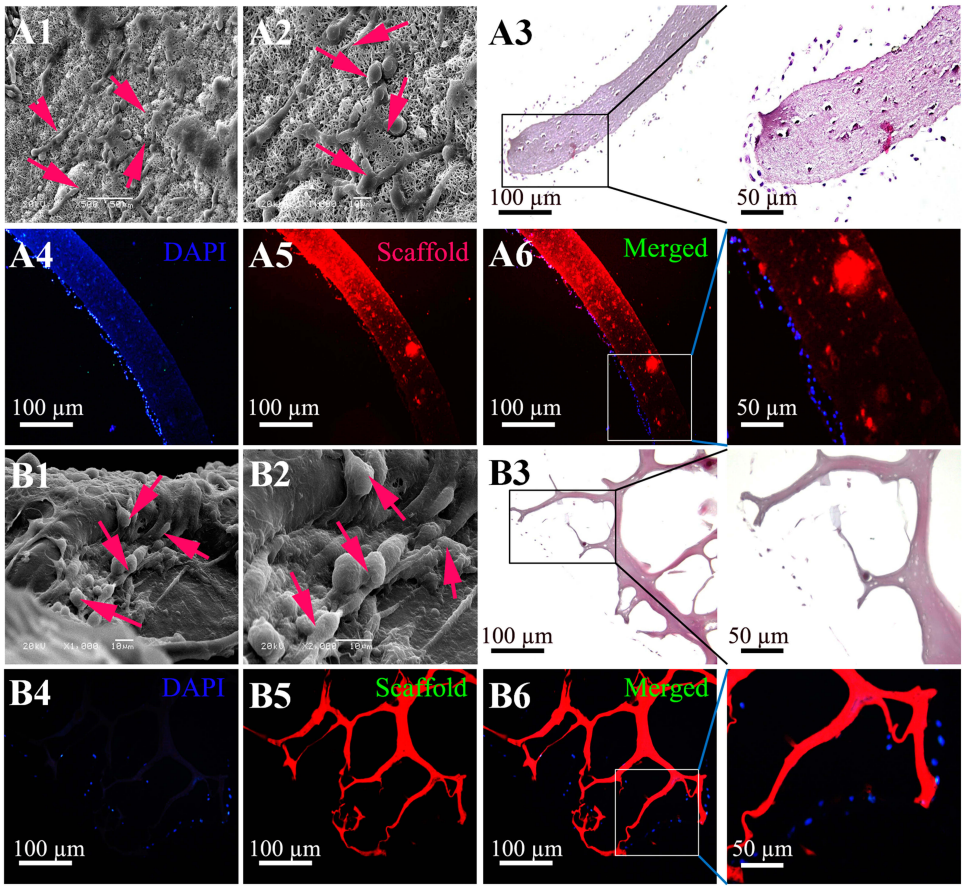

Figure 3 Adhesion and proliferation of rMSCs on the shell and core scaffolds. (**A**) Cell adhesion and proliferation on the shell scaffolds were demonstrated by SEM (**A1** and **A2**), hematoxylin and eosin (H&E) staining (**A3**) and fluorescence staining (**A4**–**A6**). (**B**) Cell adhesion and proliferation on the core scaffolds were demonstrated by SEM (**B1** and **B2**), H&E staining (**B3**) and fluorescence staining (**B4**–**B6**). Blue = DAPI staining for Nucleus. Red = scaffold (autofluorescence of genipin). Red arrows: cells. Scale bar = 100 μm.

after being cultured for 7 days is shown in Figure 3B1-B3. It was clearly found that the fusiform cells with parapodium attached on the surface of the core scaffolds. Fluorescence staining also confirmed nice cell attachment and proliferation on the shell and core scaffolds (Figure 3A4-6 and 3B4-6).

General Observations, X-Ray and CT Images for the Monitoring of Bone Formation

Tibial plateau bone defects in rabbits treated with different scaffold materials before and after 4–12 weeks of implantation are shown in Figure 4A1-3 (defect control) and 4B1-6 (CPH and CPHI). The results showed the area of bone defects in the CPHI scaffold group was significantly decreased in comparison to the CPH scaffold and defect control. The defect area in A3 was covered by connective tissue rather than the new bone tissue. This was confirmed by the H&E staining shown in Figure 6.

X-ray examination results are shown in Figure 4C. At 4 weeks after surgery, low density bone regeneration was not observed in the bone defect areas. By week 8, some high-density bone regeneration was observed in the bone defect areas in the CPH group (Figure 4C5). However, new bone formation was detected in the defect centre in the CPHI group (Figure 4C8). By 12 weeks, more high-density bone regeneration was observed in the defect site treated with the CPHI scaffolds (Figure 4C9) than that treated with the CPH composite scaffolds (Figure 4C6), indicating the formation and progression of newly formed bone towards the defect centre from peripheral edges in CPHI groups.

Three-dimensional CT reconstruction was performed for bone defects in the tibial plateau after 4–12 weeks of implantation as shown in Figure 4D1-9. The reconstructed 3D CT images directly showed newly formed bone in the defect areas. After 12 weeks of implantation, more newly

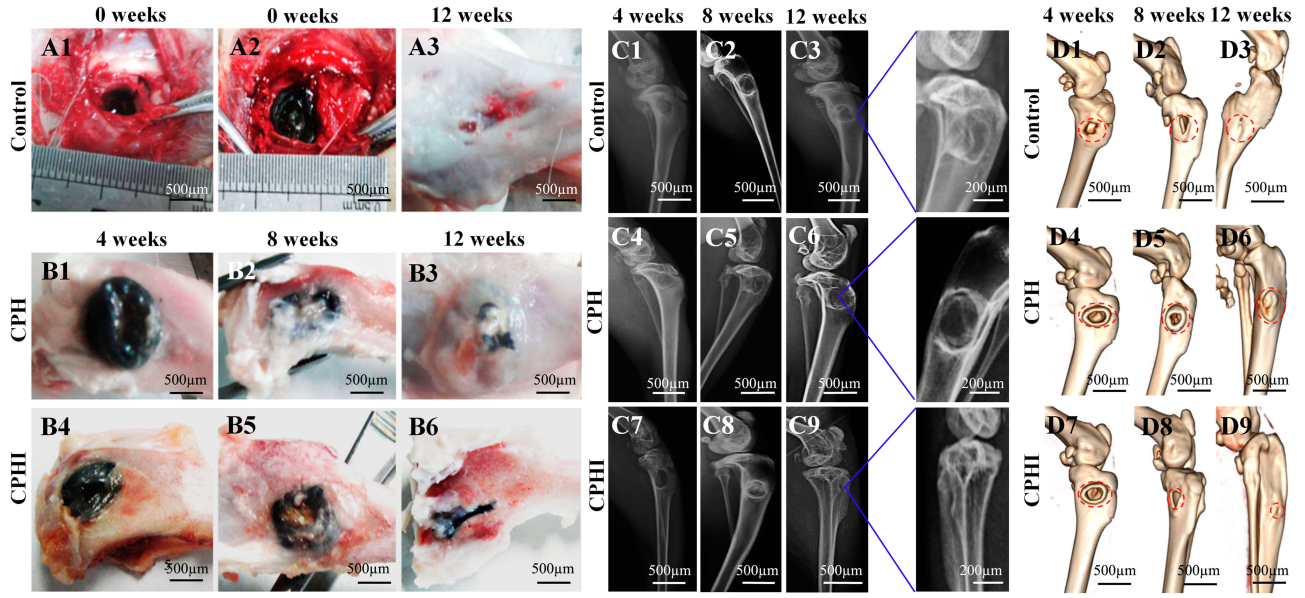

Figure 4 Implantation procedure, X-ray and 3D reconstruction analysis of new bone. (**A**) Photographs showing the surgical implantation procedure (**A1** and **A2**) of the CPH, and CPHI scaffolds in rabbit bone defects. (**A3**) shows the defect control covered by the connective tissue after 12 weeks. (**B1**–**B6**) New bone formation of CPH and CPHI groups after 4, 8, and 12 weeks. (**C1**–**C9**) Evaluation of in vivo bone formation: representative X-ray images showing the level of the regenerated bone tissue after 4–12 weeks. (**D1**–**D9**) 3D reconstruction images showed the different reparative effects of the CPH and CPHI scaffolds after 4–12 weeks. Red arrows: bone density, Red dotted circles: defect areas, Red arrow: density bone regeneration.

formed bone was observed in the area where CPHI composite scaffolds were implanted compared to that of CPH scaffolds (Figure 4D9).

Quantification of New Bone Formation (Micro-CT Scan)

Bone mineral density (BMD) and connective density (Conn.Dn) are two principal parameters for evaluating the new bone quality. The micro-CT scan was performed to quantify the new bone formation with the data shown in Figure 5. At 4 weeks, a small amount of bone-like tissue was observed within the bone defect areas (in the red circles) in the CPHI and CPH scaffold groups (Figure 5A). However, the levels of BMD (around 150 mg/cc) and Conn.Dn (less than 3.66/mm^3) was very low for all groups and also very similar between groups. By 8 weeks, bone-like tissue was observed in the CPHI and CPH groups, only accounting for 1.5±1.3% of the bone defect area in CPH group. However, BMD and Conn.Dn were markedly increased in the CPHI groups in comparison to the CPH and control groups (Figure 5A–C). At 12 weeks, more new bone formation was observed (Figure 5A) in CPHI scaffold group, evidenced by the micro-CT images and the 3D reconstruction (orange color in the right column in Figure 5A). The BMD was found around 369.9±39.67 mg/cc at 12 weeks for the CPHI group, much higher than that of CPH group (299.1±45.32 mg/cc) and control group (166.5±29.3 mg/cc) (Figure 5B). The Conn.Dn of the CPHI group (43.5 ±3.76%) at week 12 was also found significantly higher than that of CPH group (26.0±3.66%) and the control group (10.5±2.43%) (Figure 5C). These results demonstrate that CPHI scaffolds are significantly better than that of the CPH scaffolds.

New Bone Formation Assessed by Histologic Analysis

H&E staining of bone defect sites treated with CPH and CPHI composite scaffolds was carried out to evaluate their suitability as osteoinductive materials. After 4 weeks, the core of the CPHI scaffolds were filled with osteoblasts, bone matrix and immunocyte in the defect areas. Whereas, immunocyte and fibroblasts were dominating filled in the CPH scaffolds and defect groups (Figure 6A and C). By 8 weeks, new bone formation was observed and many osteoblasts appeared along with the new bone in the core of CPH and CPHI scaffolds, meanwhile, the newly-formed bone tissue were also found in the shell of the CPHI scaffolds. However, more fibrous tissue had been found in the control group (Figure 6A and C). At 12 weeks after implantation, larger amounts of bone tissue around the scaffolds and in the core scaffolds

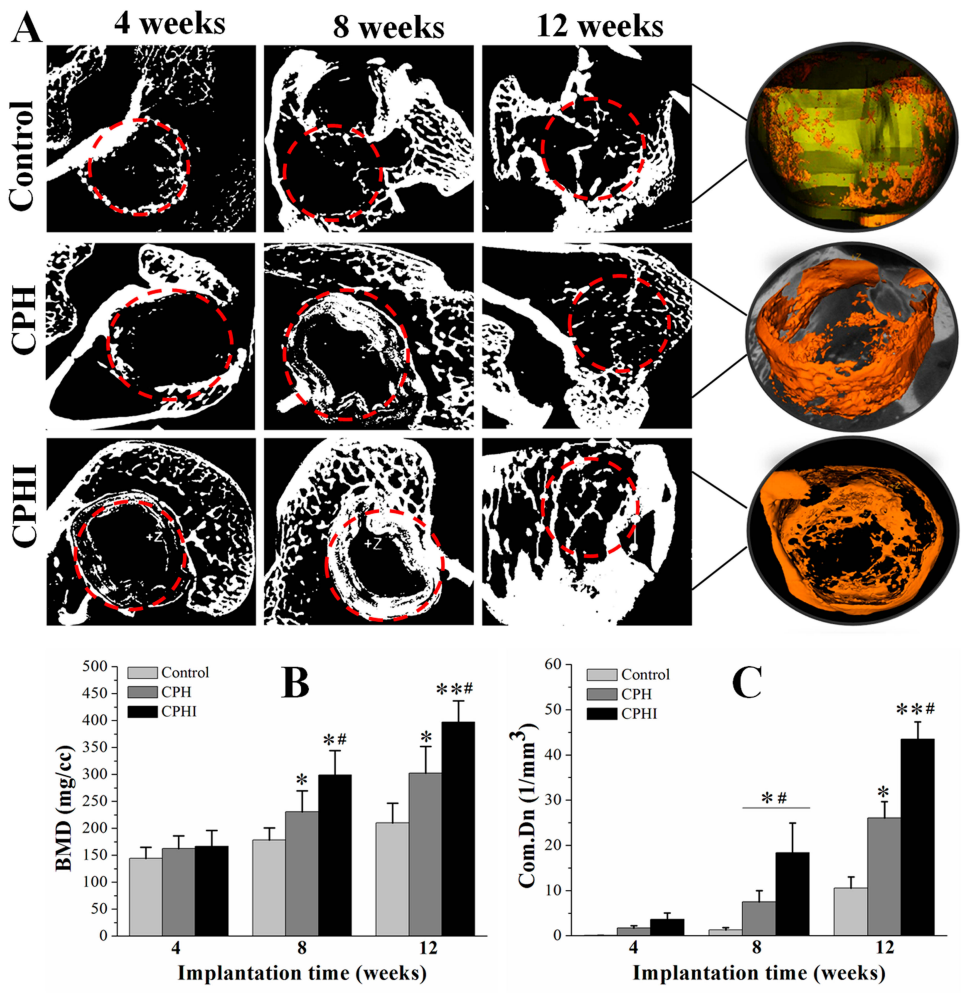

Figure 5 Micro-CT analysis of new bone. (**A**) Micro-CT scan images showing the level of regenerated bone tissue after 4–12 weeks. (**B**) Bone mineral density (BMD) of the regenerated bone tissue after 4–12 weeks. (**C**) Tissue connective density (Conn.Dn) of the regenerated bone tissue after 4–12 weeks. Data display the mean relative values calculated from three independent experiments (mean ± SD). * $p < 0.05$; ** $p < 0.01$; * is the significance compared to defect control, #is the significance compared to 8 weeks. Red dotted circles: defect areas.

were observed in the CPHI scaffold group. The shell scaffolds were also found partly degraded (Figure 6A and C).

Masson staining is shown in Figure 6B. In the fourth week, many regions had no observable bone formation in all the groups. In contrast, the core of the CPHI scaffolds were filled with fibrous tissue (blue) in the defect areas. By 8 weeks, it can be found from Figure 6B and D, large numbers of osteocytes were located in the core of the scaffolds in both of the CPH and CPHI groups. Meanwhile, mature bone tissues were also observed in the CPHI group. In contrast, the fibrous tissue filled the bone defect area of the control group at 12 weeks after implantation. In the CPHI group, abundant new bone formation was seen at 12 weeks after scaffold implantation. A similar regeneration process was observed, but only thin trabecular bone formed in the centre of the CPH scaffolds (Figure 6B and D).

Immunohistochemical Assessment

To investigate the levels of expression of alkaline phosphatase (ALP), type I collagen (COL1), osteocalcin (OC), and osteopontin (OPN), immunohistochemical staining was performed and shown in Figure 7. Four weeks after implantation, lower expression levels of COL1, OC, and OPN was observed in the CPHI group. However, positive expression of ALP was not observed. After 8 weeks, the expression of ALP, COL1, OPN and OC had markedly increased in the CPHI group, whereas low expression of ALP, COLI, OPN, and OC was detected in the CPH group, indicating the presence of cartilage tissue within the CPHI scaffolds. For both CPHI and CPH scaffold groups, the

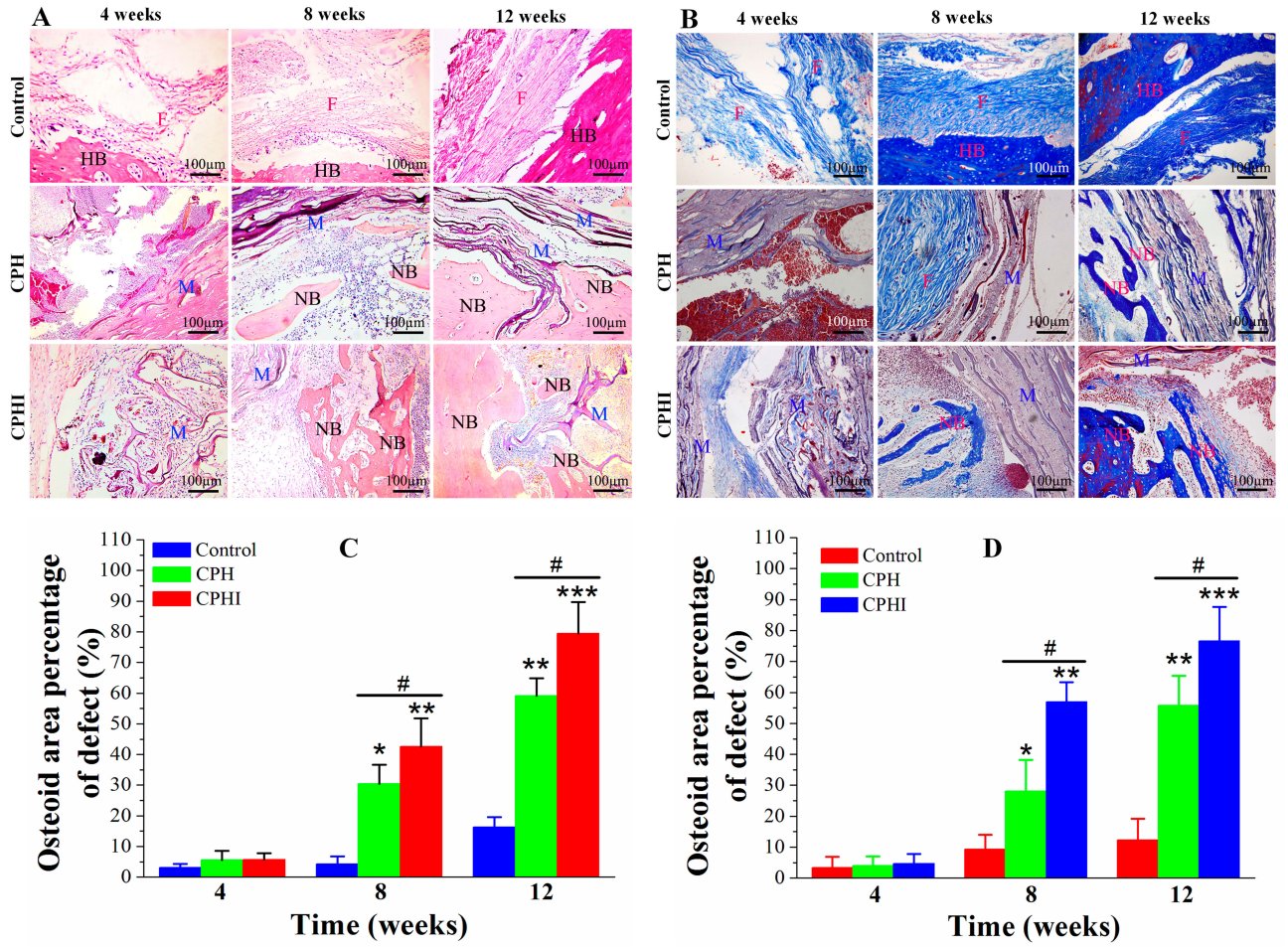

Figure 6 Histological staining assessment of the newly formed bone at 4–12 weeks post implantation of CPH and CPHI scaffolds in rabbit bone defects. **(A)** Staining with haematoxylin and eosin (H&E) demonstrates new bone formed in the CPH and CPHI scaffolds. **(B)** Masson's trichrome shows matrix distribution (scale bar = 100 μm). (**C**) and (**D**) Show the quantitative data from (**A**) and (**B**), respectively. Data display the mean relative values calculated from three independent experiments (mean ± SD). * $p < 0.05$; ** $p < 0.01$; *** $p < 0.001$; * is the significance compared to defect control, # $p < 0.05$; is the significance compared to CPH group.
Abbreviations: NB, new bone; M, implanted material; HB, host bone; F, fibrous tissue.

intensity of positive staining for COL1, OPN, and OC increased with time and the expression was mainly seen in the new bone. However, the expression levels of these proteins in the CPH group were much less than that in the CPHI groups (Figure 7A–H).

Discussion

In this study, we fabricated the core-shell composite scaffolds with ICA-loaded chitosan microspheres incorporated into collagen 1 as core scaffolds and polycaprolactone/collagen/hydroxyapatite (CPH) composite was used to prepare the shell scaffolds by electrospinning (Figure 1A and B). Our aim is to evaluate whether this new-type of scaffolds can remarkably promote bone regeneration. Previous study showed that ICA not only can induce MSCs to differentiate into osteoblasts but also promote osteogenesis,[51,52] meanwhile, Xie et al[30] studied the effect of ICA-SF/PLCL nanofibrous membrane by coaxial electrospinning on bone regeneration. The results showed that ICA-SF/PLCL nanofibrous membrane can promote bone regeneration. Zhang et al[53] also reported that the calcinated antler cancellous bone (CACB) scaffolds with ICA, not only increased osteogenic gene expression, mineralization of rat bone marrow mesenchymal stem cells but also promoted the osteogenesis and neovascularization both in vitro and in vivo. All these results indicated that ICA as a bioactive factor has a potential value for BTE. However, the use of ICA in scaffolds for bone regeneration has not been well studied. MSCs homing is an inchoate event in the injured tissue. ICA plays an important role in MSCs homing, which is a vital mechanism of tissue regeneration.[54] Based on these factors, we fabricated

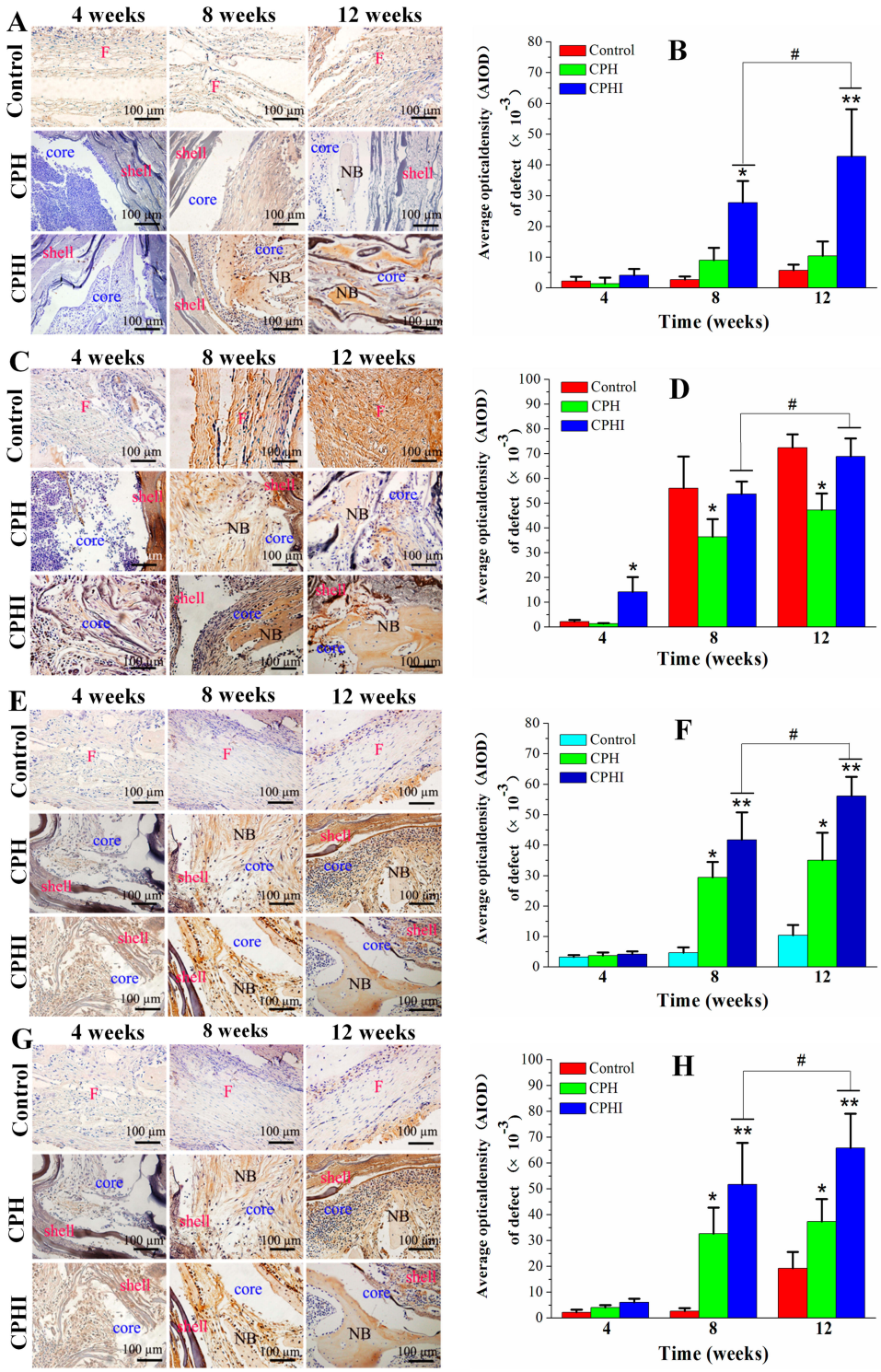

Figure 7 Immunohistochemistry staining for (**A**) alkaline phosphatase (ALP), (**C**) type I collagen (COL1), (**E**) osteocalcin (OC), and (**G**) osteopontin (OPN) of bone defects at 4–12 weeks post implantation in rabbits. (**B**), (**D**), (**F**), and (**H**) Show the quantitative data from (**A**), (**C**), (**E**), and (**G**), respectively. Data display the mean relative values calculated from three independent experiments (mean ± SD). * $p < 0.05$; ** $p < 0.01$; * is the significance compared to defect control, # $p < 0.05$; is the significance compared to CPH group. Scale bar = 100 μm.

Abbreviations: NB, new bone; F, fibrous tissue.

a new core-shell scaffold that not only release ICA in early stage of bone regeneration, but also maintained new bone formation.

An Ideal scaffold for bone repair should be able to mimic the natural extracellular matrix.[55,56] In this study, we chose type 1 collagen, HA and PCL as the main

components for electrospinning to fabricate the shell of the composite scaffolds (Figure 1A and B). This is because type 1 collagen is one of the main components of bone and also has excellent biocompatibility with no toxicity and no immunogenicity. It can also support and protect cells, and mediate cell adhesion.[57] PCL is a resorbable polymer that has a much lower rate of degradation and excellent mechanical properties.[58] HA is also a main natural component of bone, which had been applied in BTE for long time.[59,60] For example, Fu et al[61] fabricated the composite scaffold composed of poly(ε-caprolactone)-poly(ethylene glycol)-poly(ε-caprolactone) (PCL-PEG-PCL, PCEC) and 30 wt.% nano-hydroxyapatite (n-HA) through electrospinning, and showed excellent activity in guiding bone regeneration. Several investigators have developed the electrospun PCL/COL/HA scaffolds in promoting bone regeneration. For example, Phipps MC. Fabricated the scaffolds composed of blended PCL/collagen I nanofibers, and nanoparticles of HA, promoted greater mesenchymal stem cell (MSC) adhesion, and proliferation, as compared with scaffolds composed of PCL alone.[62] Therefore, the PCL/COL/HA scaffolds have potential utility as a substrates for supporting cell expanded and tissue regeneration. Based on electrospun scaffolds have nanofibrous structure, large surface to volume ratio, and interconnecting pores, therefore, its has potential utility in bone repair. However, the small pore sizes in electrospun scaffolds constrain cell growth and tissue-ingrowth. In order to overcome this drawback, several strategies have been developed for increasing the average pore size of the electrospun scaffolds. Pham et al resolved this issue by decreasing layers of nanofibers.[63] Others reported that the electrospun scaffolds were fabricated by salt leaching[64] or cryogenic electrospinning.[65] Some investigators have explored co-electrospinning sacrificial fibers along with stable fibers, the larger pores were created when the sacrificial fibers removed, the cells successful infiltrated in the scaffold.[66] Core-shell structured nanofibers as a promising material were fabricated by the coaxial electrospinning technique, which could promote osteoblast cell growth in bone tissue engineering.[67] However, the key problem of these strategies is the pores sizes not adequate to enhance cellular infiltration. Therefore, it is tickler for the electrospun scaffolds that how to mimic native bone increase bone tissue regeneration.

In this study, a new strategy was employed to construct shell scaffold using PCL/COL/HA materials through electrospinning. Meanwhile, the amount of HA was gradually increased from interior to outer layer of the shell scaffolds, which mimic the natural cortical bone structure. On the other hand, ICA-loaded microspheres were incorporated into the core scaffold. Due to the easy degradation of collagen, ICA can rapidly release in the early stage and plays its role in early bone regeneration (Figure 2B).

The mechanical strength of the scaffold plays a crucial role in BTE.[68,69] In order to increase the mechanical strength of the scaffolds, we employed genipin as a cross-linking agent to treat the core-shell scaffolds. Mechanical strength of the scaffolds was remarkably increased after scaffolds were cross-linked[70] (Figure 1F). Meanwhile, the degradation rate of the scaffold was decreased (Figure 1E). Degradation speed of the scaffold is one of the important factors for BTE. Fast degradation of the scaffold results in the lack of mechanical support during the new tissue forming, while slow degradation of the scaffold results in the inflammatory response, impairing new tissue regeneration.[71] Therefore, controlled biodegradability is essential for the scaffolds in BTE. Our results showed that the degradation behaviour of the cross-linked scaffolds was significantly decreased in comparison with the uncross-linked scaffolds, providing a controlled biodegradability suitable for bone defect regeneration (Figure 1E).

Pore sizes are important for BTE scaffolds and has been shown to affect the progression of osteogenesis.[72] Small pore size (< 100 μm) not only reduce cell migration but also restrict nutrient delivery and waste removal. Additionally, it also limit the amount of new tissue regeneration.[72] It has been reported that pore size > 100 μm with gradients are recommended.[73,74] We had fabricated the core-shell CPH and CPHI scaffolds by electrospinning and freeze drying with a gradient in pore sizes to facilitate the repair of tibia bone defects in rabbit models. SEM images confirmed the gradients of pore sizes in scaffolds (Figure 2A and B). The active ingrowth of bone inside the scaffolds can be attributed to the fully interconnected pores (Figure 3). The radiography, micro-CT, H&E and Masson staining results indicate that the amount of bone formation in the CPHI group was markedly higher than those in other groups. The formation of new bone can also increase collagen synthesis and mineralization in the period of bone regeneration (Figures 4–6). The results demonstrated that both CPH and CPHI scaffolds provided adequate pores for cellular attachment and proliferation in vivo.

Immunohistochemistry results showed that the biomarkers of osteogenesis, including ALP, COL1, OCN and

OPN, were markedly increased in the CPHI group compared with the CPH group for weeks 8 and 12 (Figure 7). This indicates that the sustained release of ICA from CPHI scaffolds remarkably promoted new bone formation without adverse effects. These results indicate that the CPHI scaffolds have excellent osteoinductivity and osteoconductivity. The distinct features of the scaffolds may explain this superior therapeutic efficacy: Firstly, since the core scaffolds were loaded with ICA and shell scaffolds were combined with HA, excellent osteoinductivity was achieved due to the synergistic effect of ICA and HA on increasing bone tissue regeneration.[75] Secondly, the highly ordered channel structure with gradients of pore sizes provided a suitable space for local bone remodelling initiated by stimulating the proliferation of osteoblasts and recruiting osteoprogenitors to defect location.[76] Finally, the degradation rate of CPH scaffold nicely matches the bone formation rate at the defect site,[77] ensuring the scaffold degradation give way to newly secreted bone matrix and sequential mineralization.

Conclusion

In this study, two types of scaffolds (CPH and CPHI) were fabricated through electrospinning and freeze-drying technologies and implanted into rabbits for up to 12 weeks. ICA was loaded into the core scaffolds to form the CPHI scaffolds. X-ray, micro-CT, histological, and histochemical methods were employed to study the bone regeneration processes. X-ray image showed changes of the lamina bony defect over time. In the CPH scaffolds group, the bony defect was not completely filled even at week 12 due to the lack of new bone formation. On the other hand, at both weeks 8 and 12, the bony defects in the CPHI scaffolds group were filled with a bone mass with the progression of the new bone formation being clearly seen from the X-ray images at weeks 8 and 12. Much denser bone with better lamina reconstruction was observed. Meanwhile, the bone formation of the CPHI and CPH groups was also analysed by histological method with H&E and Masson staining. There was no noticeable new bone formation inside the scaffolds of the control and CPH groups at week 4. On the other hand, active new bone formation was observed around the scaffold and even in the centre of the CPHI group. Little new bone formation was observed in the scaffolds area in CPH group at week 8. Whereas in CPHI group, a substantial amount of new bone was observed in the interface between the ulna and radius. Ingrowth of new bone inside the scaffolds was also found. At week 12, calcified and matured new bone that infiltrated into the scaffolds was observed in both CPH and CPHI groups. However, CPHI scaffolds were found more effective than CPH scaffolds in inducing bone regeneration. This was due to the fact that ICA release from CPHI increased cell growth and differentiation, together with the synergetic effect of HA, making the scaffolds more osteoinductive than CPH scaffolds. These results suggested that CPHI scaffolds have great potential for the induction of bone regeneration and application in tissue engineering of bone defects repair.

Acknowledgments

We gratefully acknowledge funding from the Key Project of Science and Technology of Jiangsu Province (Grant BE2018644) and the major projects of science and technology in Gansu Province (Grant 1203FKDA036). We gratefully acknowledge Changzhou Second People's Hospital Affiliated to Nanjing Medical University for support. XZ also thanks the Jiangsu specially-appointed professors program for support.

Disclosure

The authors report no conflicts of interest in this work.

References

1. Fernandez de Grado G, Keller L, Idoux-Gillet Y, et al. Bone substitutes: a review of their characteristics, clinical use, and perspectives for large bone defects management. *J Tissue Eng*. 2018;9:2041731418776819. doi:10.1177/2041731418776819
2. Stevenson S. Enhancement of fracture healing with autogenous and allogeneic bone grafts. *Clin Orthop Relat Res*. 1998;355S(355 Suppl):S239–246. doi:10.1097/00003086-199810001-00024
3. Ghayor C, Weber FE. Osteoconductive microarchitecture of bone substitutes for bone regeneration revisited. *Front Physiol*. 2018;9:960. doi:10.3389/fphys.2018.00960
4. Salgado AJ, Coutinho OP, Reis RL. Bone tissue engineering: state of the art and future trends. *Macromol Biosci*. 2004;4(8):743–765. doi:10.1002/mabi.200400026
5. Jimi E, Hirata S, Osawa K, Terashita M, Kitamura C, Fukushima H. The current and future therapies of bone regeneration to repair bone defects. *Int J Dent*. 2012;2012:148261. doi:10.1155/2012/148261
6. Heydari Z, Mohebbi-Kalhori D, Afarani MS. Engineered electrospun polycaprolactone (PCL)/octacalcium phosphate (OCP) scaffold for bone tissue engineering. *Mater Sci Eng C Mater Biol Appl*. 2017;81:127–132. doi:10.1016/j.msec.2017.07.041
7. Luo W, Zhang S, Lan Y, et al. 3D printed porous polycaprolactone/oyster shell powder (PCL/OSP) scaffolds for bone tissue engineering. *Mater Res Express*. 2018;5(4):045403. doi:10.1088/2053-1591/aab916
8. Cunniffe GM, Curtin CM, Thompson EM, Dickson GR, O'Brien FJ. Content-dependent osteogenic response of nanohydroxyapatite: an in vitro and in vivo assessment within collagen-based scaffolds. *ACS Appl Mater Interfaces*. 2016;8(36):23477–23488. doi:10.1021/acsami.6b06596

9. Xu T, Miszuk JM, Zhao Y, Sun H, Fong H. Electrospun polycaprolactone 3D nanofibrous scaffold with interconnected and hierarchically structured pores for bone tissue engineering. *Adv Healthc Mater*. 2015;4(15):2238–2246. doi:10.1002/adhm.201500345
10. Shkarina S, Shkarin R, Weinhardt V, et al. 3D biodegradable scaffolds of polycaprolactone with silicate-containing hydroxyapatite microparticles for bone tissue engineering: high-resolution tomography and in vitro study. *Sci Rep*. 2018;8(1):8907. doi:10.1038/s41598-018-27097-7
11. Zou L, Zhang Y, Liu X, Chen J, Zhang Q. Biomimetic mineralization on natural and synthetic polymers to prepare hybrid scaffolds for bone tissue engineering. *Colloids Surf B Biointerfaces*. 2019;178:222–229. doi:10.1016/j.colsurfb.2019.03.004
12. Clarke B. Normal bone anatomy and physiology. *Clin J Am Soc Nephrol*. 2008;3(Suppl 3):S131–139. doi:10.2215/CJN.04151206
13. Tierney CM, Haugh MG, Liedl J, Mulcahy F, Hayes B, O'Brien FJ. The effects of collagen concentration and crosslink density on the biological, structural and mechanical properties of collagen-GAG scaffolds for bone tissue engineering. *J Mech Behav Biomed Mater*. 2009;2(2):202–209. doi:10.1016/j.jmbbm.2008.08.007
14. Filardo G, Kon E, Tampieri A, et al. New bio-ceramization processes applied to vegetable hierarchical structures for bone regeneration: an experimental model in sheep. *Tissue Eng Part A*. 2014;20(3–4):763–-773. doi:10.1089/ten.TEA.2013.0108
15. Hayrapetyan A, Bongio M, Leeuwenburgh SC, Jansen JA, van den Beucken JJ. Effect of nano-HA/collagen composite hydrogels on osteogenic behavior of mesenchymal stromal cells. *Stem Cell Rev*. 2016;12(3):352–364. doi:10.1007/s12015-016-9644-x
16. Wang C, Zhao Q, Wang M. Cryogenic 3D printing for producing hierarchical porous and rhBMP-2-loaded Ca-P/PLLA nanocomposite scaffolds for bone tissue engineering. *Biofabrication*. 2017;9(2):025031. doi:10.1088/1758-5090/aa71c9
17. Cao H, Kuboyama N. A biodegradable porous composite scaffold of PGA/beta-TCP for bone tissue engineering. *Bone*. 2010;46(2):386–395. doi:10.1016/j.bone.2009.09.031
18. Yao Q, Cosme JG, Xu T, et al. Three dimensional electrospun PCL/PLA blend nanofibrous scaffolds with significantly improved stem cells osteogenic differentiation and cranial bone formation. *Biomaterials*. 2017;115:115–127. doi:10.1016/j.biomaterials.2016.11.018
19. Lai Y, Li Y, Cao H, et al. Osteogenic magnesium incorporated into PLGA/TCP porous scaffold by 3D printing for repairing challenging bone defect. *Biomaterials*. 2019;197:207–219. doi:10.1016/j.biomaterials.2019.01.013
20. Luo JW, Liu C, Wu JH, et al. In situ forming gelatin/hyaluronic acid hydrogel for tissue sealing and hemostasis. *J Biomed Mater Res B Appl Biomater*. 2019.
21. Zein I, Hutmacher DW, Tan KC, Teoh SH. Fused deposition modeling of novel scaffold architectures for tissue engineering applications. *Biomaterials*. 2002;23(4):1169–1185. doi:10.1016/S0142-9612(01)00232-0
22. Jung MR, Shim IK, Chung HJ, et al. Local BMP-7 release from a PLGA scaffolding-matrix for the repair of osteochondral defects in rabbits. *J Controlled Release*. 2012;162(3):485–491. doi:10.1016/j.jconrel.2012.07.040
23. Nielsen EO, Chen L, Hansen JO, Degn M, Overgaard S, Ding M. Optimizing osteogenic differentiation of ovine adipose-derived stem cells by osteogenic induction medium and FGFb, BMP2, or NELL1 in vitro. *Stem Cells Int*. 2018;2018:9781393. doi:10.1155/2018/9781393
24. Eap S, Keller L, Schiavi J, et al. A living thick nanofibrous implant bifunctionalized with active growth factor and stem cells for bone regeneration. *Int J Nanomedicine*. 2015;10:1061–1075. doi:10.2147/IJN.S72670
25. Mitsak AG, Kemppainen JM, Harris MT, Hollister SJ. Effect of polycaprolactone scaffold permeability on bone regeneration in vivo. *Tissue Eng Part A*. 2011;17(13–14):1831–1839. doi:10.1089/ten.tea.2010.0560
26. Rashad A, Mohamed-Ahmed S, Ojansivu M, et al. Coating 3D printed polycaprolactone scaffolds with nanocellulose promotes growth and differentiation of mesenchymal stem cells. *Biomacromolecules*. 2018;19(11):4307–4319. doi:10.1021/acs.biomac.8b01194
27. Martino S, D'Angelo F, Armentano I, Kenny JM, Orlacchio A. Stem cell-biomaterial interactions for regenerative medicine. *Biotechnol Adv*. 2012;30(1):338–351. doi:10.1016/j.biotechadv.2011.06.015
28. Zhang D, Wu X, Chen J, Lin K. The development of collagen based composite scaffolds for bone regeneration. *Bioactive Mater*. 2018;3(1):129–138. doi:10.1016/j.bioactmat.2017.08.004
29. Zhang L, Zhang X, Li KF, et al. Icariin promotes extracellular matrix synthesis and gene expression of chondrocytes in vitro. *Phytother Res*. 2012;26(9):1385–1392. doi:10.1002/ptr.3733
30. Xie X, Pei F, Wang H, Tan Z, Yang Z, Kang P. Icariin: a promising osteoinductive compound for repairing bone defect and osteonecrosis. *J Biomater Appl*. 2015;30(3):290–299. doi:10.1177/0885328215581551
31. He J-P, Feng X, Wang J-F, et al. Icariin prevents bone loss by inhibiting bone resorption and stabilizing bone biological apatite in a hindlimb suspension rodent model. *Acta Pharmacol Sin*. 2018;39(11):1760–1767. doi:10.1038/s41401-018-0040-8
32. Wang Z, Li K, Sun H, Wang J, Fu Z, Liu M. Icariin promotes stable chondrogenic differentiation of bone marrow mesenchymal stem cells in selfassembling peptide nanofiber hydrogel scaffolds. *Mol Med Rep*. 2018;17(6):8237–8243. doi:10.3892/mmr.2018.8913
33. Venkatesan J, Kim SK. Chitosan composites for bone tissue engineering–an overview. *Mar Drugs*. 2010;8(8):2252–2266. doi:10.3390/md8082252
34. Thein-Han WW, Misra RD. Biomimetic chitosan-nanohydroxyapatite composite scaffolds for bone tissue engineering. *Acta Biomater*. 2009;5(4):1182–1197. doi:10.1016/j.actbio.2008.11.025
35. Sinha VR, Singla AK, Wadhawan S, et al. Chitosan microspheres as a potential carrier for drugs. *Int J Pharm*. 2004;274(1–2):1–33. doi:10.1016/j.ijpharm.2003.12.026
36. Liu H, Zhu J, Bao P, et al. Construction and in vivo/in vitro evaluation of a nanoporous ion-responsive targeted drug delivery system for recombinant human interferon alpha-2b delivery. *Int J Nanomedicine*. 2019;14:5339–5353. doi:10.2147/IJN.S209646
37. Feng C, Wang Z, Jiang C, et al. Chitosan/o-carboxymethyl chitosan nanoparticles for efficient and safe oral anticancer drug delivery: in vitro and in vivo evaluation. *Int J Pharm*. 2013;457(1):158–167. doi:10.1016/j.ijpharm.2013.07.079
38. Zhang H, Fu QW, Sun TW, et al. Amorphous calcium phosphate, hydroxyapatite and poly(d,l-lactic acid) composite nanofibers: electrospinning preparation, mineralization and in vivo bone defect repair. *Colloids Surf B Biointerfaces*. 2015;136:27–36. doi:10.1016/j.colsurfb.2015.08.015
39. Wu J, Hong Y. Enhancing cell infiltration of electrospun fibrous scaffolds in tissue regeneration. *Bioactive Mater*. 2016;1(1):56–64. doi:10.1016/j.bioactmat.2016.07.001
40. Zhou Y, Chyu J, Zumwalt M. Recent progress of fabrication of cell scaffold by electrospinning technique for articular cartilage tissue engineering. *Int J Biomater*. 2018;2018:1953636. doi:10.1155/2018/1953636
41. Xin X, Hussain M, Mao JJ. Continuing differentiation of human mesenchymal stem cells and induced chondrogenic and osteogenic lineages in electrospun PLGA nanofiber scaffold. *Biomaterials*. 2007;28(2):316–325. doi:10.1016/j.biomaterials.2006.08.042
42. Zafar M, Najeeb S, Khurshid Z, et al. Potential of electrospun nanofibers for biomedical and dental applications. *Materials (Basel)*. 2016;9:2. doi:10.3390/ma9020073
43. Nerurkar NL, Sen S, Baker BM, Elliott DM, Mauck RL. Dynamic culture enhances stem cell infiltration and modulates extracellular matrix production on aligned electrospun nanofibrous scaffolds. *Acta Biomater*. 2011;7(2):485–491. doi:10.1016/j.actbio.2010.08.011

44. Milleret V, Simona B, Neuenschwander P, Hall H. Tuning electrospinning parameters for production of 3D-fiber-fleeces with increased porosity for soft tissue engineering applications. *Eur Cell Mater*. 2011;21:286–303. doi:10.22203/eCM.v021a22
45. Ekaputra AK, Prestwich GD, Cool SM, Hutmacher DW. Combining electrospun scaffolds with electrosprayed hydrogels leads to three-dimensional cellularization of hybrid constructs. *Biomacromolecules*. 2008;9(8):2097–2103. doi:10.1021/bm800565u
46. Lewandowska-Lancucka J, Gilarska A, Bula A, Horak W, Latkiewicz A, Nowakowska M. Genipin crosslinked bioactive collagen/chitosan/hyaluronic acid injectable hydrogels structurally amended via covalent attachment of surface-modified silica particles. *Int J Biol Macromol*. 2019;136:1196–1208. doi:10.1016/j.ijbiomac.2019.06.184
47. Mahmood SK, Zakaria M, Razak I, et al. Preparation and characterization of cockle shell aragonite nanocomposite porous 3D scaffolds for bone repair. *Biochem Biophys Rep*. 2017;10:237–251. doi:10.1016/j.bbrep.2017.04.008
48. Xiao H, Huang W, Xiong K, et al. Osteochondral repair using scaffolds with gradient pore sizes constructed with silk fibroin, chitosan, and nano-hydroxyapatite. *Int J Nanomedicine*. 2019;14:2011–2027. doi:10.2147/IJN.S191627
49. Diaz E, Puerto I, Ribeiro S, Lanceros-Mendez S, Barandiaran JM. The influence of copolymer composition on PLGA/nHA scaffolds' cytotoxicity and in vitro degradation. *Nanomaterials (Basel, Switzerland)*. 2017;7:7. doi:10.3390/nano7120458
50. Chen D, Zhu T, Fu W, Zhang H. Electrospun polycaprolactone/collagen nanofibers cross-linked with 1-ethyl-3-(3-dimethylaminopropyl) carbodiimide/N-hydroxysuccinimide and genipin facilitate endothelial cell regeneration and may be a promising candidate for vascular scaffolds. *Int J Nanomedicine*. 2019;14:2127–2144. doi:10.2147/IJN.S192699
51. Yang A, Yu C, Lu Q, Li H, Li Z, He C. Mechanism of action of icariin in bone marrow mesenchymal stem cells. *Stem Cells Int*. 2019;2019:5747298. doi:10.1155/2019/5747298
52. Fan JJ, Cao LG, Wu T, et al. The dose-effect of icariin on the proliferation and osteogenic differentiation of human bone mesenchymal stem cells. *Molecules*. 2011;16(12):10123–10133. doi:10.3390/molecules161210123
53. Zhang X, Xu M, Song L, et al. Effects of compatibility of deproteinized antler cancellous bone with various bioactive factors on their osteogenic potential. *Biomaterials*. 2013;34(36):9103–9114. doi:10.1016/j.biomaterials.2013.08.024
54. De Becker A, Riet IV. Homing and migration of mesenchymal stromal cells: how to improve the efficacy of cell therapy? *World J Stem Cells*. 2016;8(3):73–87. doi:10.4252/wjsc.v8.i3.73
55. Sprio S, Fricia M, Maddalena GF, Nataloni A, Tampieri A. Osteointegration in cranial bone reconstruction: a goal to achieve. *J Appl Biomater Funct Mater*. 2016;14(4):e470–e476. doi:10.5301/jabfm.5000293
56. Dennis SC, Berkland CJ, Bonewald LF, Detamore MS. Endochondral ossification for enhancing bone regeneration: converging native extracellular matrix biomaterials and developmental engineering in vivo. *Tissue Eng Part B Rev*. 2015;21(3):247–266. doi:10.1089/ten.teb.2014.0419
57. Delgado LM, Fuller K, Zeugolis DI. Collagen cross-linking: biophysical, biochemical, and biological response analysis. *Tissue Eng Part A*. 2017;23(19–20):1064–1077. doi:10.1089/ten.tea.2016.0415
58. Hutmacher DW, Schantz T, Zein I, Ng KW, Teoh SH, Tan KC. Mechanical properties and cell cultural response of polycaprolactone scaffolds designed and fabricated via fused deposition modeling. *J Biomed Mater Res*. 2001;55(2):203–216. doi:10.1002/1097-4636(200105)55:2<203::AID-JBM1007>3.0.CO;2-7
59. A A, Menon D, BS T, et al. Bioinspired composite matrix containing hydroxyapatite-silica core-shell nanorods for bone tissue engineering. *ACS Appl Mater Interfaces*. 2017;9(32):26707–26718. doi:10.1021/acsami.7b07131
60. Na K, Kim SW, Sun BK, et al. Osteogenic differentiation of rabbit mesenchymal stem cells in thermo-reversible hydrogel constructs containing hydroxyapatite and bone morphogenic protein-2 (BMP-2). *Biomaterials*. 2007;28(16):2631–2637. doi:10.1016/j.biomaterials.2007.02.008
61. Fu S, Ni P, Wang B, et al. In vivo biocompatibility and osteogenesis of electrospun poly(epsilon-caprolactone)-poly(ethylene glycol)-poly(epsilon-caprolactone)/nano-hydroxyapatite composite scaffold. *Biomaterials*. 2012;33(33):8363–8371. doi:10.1016/j.biomaterials.2012.08.023
62. Phipps MC, Clem WC, Catledge SA, et al. Mesenchymal stem cell responses to bone-mimetic electrospun matrices composed of polycaprolactone, collagen I and nanoparticulate hydroxyapatite. *PLoS One*. 2011;6(2):e16813. doi:10.1371/journal.pone.0016813
63. Pham QP, Sharma U, Mikos AG. Electrospun poly(epsilon-caprolactone) microfiber and multilayer nanofiber/microfiber scaffolds: characterization of scaffolds and measurement of cellular infiltration. *Biomacromolecules*. 2006;7(10):2796–2805. doi:10.1021/bm060680j
64. Nam J, Huang Y, Agarwal S, Lannutti J. Improved cellular infiltration in electrospun fiber via engineered porosity. *Tissue Eng*. 2007;13(9):2249–2257. doi:10.1089/ten.2006.0306
65. Leong MF, Rasheed MZ, Lim TC, Chian KS. In vitro cell infiltration and in vivo cell infiltration and vascularization in a fibrous, highly porous poly(D,L-lactide) scaffold fabricated by cryogenic electrospinning technique. *J Biomed Mater Res A*. 2009;91(1):231–240. doi:10.1002/jbm.a.32208
66. Phipps MC, Clem WC, Grunda JM, Clines GA, Bellis SL. Increasing the pore sizes of bone-mimetic electrospun scaffolds comprised of polycaprolactone, collagen I and hydroxyapatite to enhance cell infiltration. *Biomaterials*. 2012;33(2):524–534. doi:10.1016/j.biomaterials.2011.09.080
67. Chen P, Liu L, Pan J, Mei J, Li C, Zheng Y. Biomimetic composite scaffold of hydroxyapatite/gelatin-chitosan core-shell nanofibers for bone tissue engineering. *Mater Sci Eng C Mater Biol Appl*. 2019;97:325–335. doi:10.1016/j.msec.2018.12.027
68. Temenoff JS, Mikos AG. Review: tissue engineering for regeneration of articular cartilage. *Biomaterials*. 2000;21(5):431–440. doi:10.1016/S0142-9612(99)00213-6
69. Hutmacher DW. Scaffolds in tissue engineering bone and cartilage. *Biomaterials*. 2000;21(24):2529–2543. doi:10.1016/S0142-9612(00)00121-6
70. Lu H-T, Lu T-W, Chen C-H, Mi F-L. Development of genipin-crosslinked and fucoidan-adsorbed nano-hydroxyapatite/hydroxypropyl chitosan composite scaffolds for bone tissue engineering. *Int J Biol Macromol*. 2019;128:973–984. doi:10.1016/j.ijbiomac.2019.02.010
71. Mountziaris PM, Mikos AG. Modulation of the inflammatory response for enhanced bone tissue regeneration. *Tissue Eng Part B Rev*. 2008;14(2):179–186. doi:10.1089/ten.teb.2008.0038
72. Karageorgiou V, Kaplan D. Porosity of 3D biomaterial scaffolds and osteogenesis. *Biomaterials*. 2005;26(27):5474–5491. doi:10.1016/j.biomaterials.2005.02.002
73. Song W, Yu X, Markel DC, Shi T, Ren W. Coaxial PCL/PVA electrospun nanofibers: osseointegration enhancer and controlled drug release device. *Biofabrication*. 2013;5(3):035006. doi:10.1088/1758-5082/5/3/035006
74. Zhang X, Chang W, Lee P, et al. Polymer-ceramic spiral structured scaffolds for bone tissue engineering: effect of hydroxyapatite composition on human fetal osteoblasts. *PLoS One*. 2014;9(1):e85871. doi:10.1371/journal.pone.0085871
75. Yang J, Liu Y, He L, et al. Icariin conjugated hyaluronic acid/collagen hydrogel for osteochondral interface restoration. *Acta Biomater*. 2018;74:156–167. doi:10.1016/j.actbio.2018.05.005

76. Huang Y, Shi R, Gong M, et al. Icariin-loaded electrospun PCL/gelatin sub-microfiber mat for preventing epidural adhesions after laminectomy. *Int J Nanomedicine*. 2018;13:4831–4844. doi:10.2147/IJN.S169427

77. Shirazi RN, Ronan W, Rochev Y, McHugh P. Modelling the degradation and elastic properties of poly(lactic-co-glycolic acid) films and regular open-cell tissue engineering scaffolds. *J Mech Behav Biomed Mater*. 2016;54:48–59. doi:10.1016/j.jmbbm.2015.08.030